



Nonlinear alternating current conduction study in manganese-doped zinc oxide nanocapsules and nanoplates

Amit Kumar Bhunia¹ · Tilak Narayan Ghosh² · Khokan Bhunia³ · Satyajit Saha⁴

Received: 25 November 2022 / Accepted: 27 December 2022 / Published online: 9 January 2023
© The Author(s), under exclusive licence to Springer-Verlag GmbH, DE part of Springer Nature 2023

Abstract

In this report, the real part of ac conductance ($\Sigma(T, f)$) of pure ZnO nanoparticle, manganese-doped ZnO nanocapsules and nanoplates was estimated as a component of frequency (f) by shifting zero-frequency Ohmic conductance (Σ_0) with the tuning of the temperature (T) to understand the nonlinear AC conduction mechanism in semiconductor. The UV–VIS absorption spectrum showed a change in band gap from 3.67 eV for pure ZnO NPs to 3.31 eV for Mn-doped ZnO NPs with the change in excitonic peak from 372.5 nm for ZnO NPs to 375 nm for Mn-ZnO NPs. The HRTEM and SAED analysis along with XRD showed formation of nanocapsules and nanoplates with hexagonal wurtzite crystal phase. The doped semiconductor nanocrystals showed a ‘ T ’ dependent transition nature. Scaling speculations from theoretical models are used to dissect the effects of ac conduction and the nonlinearity exponent (x_f) of the onset frequency $f_c \sim \Sigma_0^{x_f}$. The overall scaling formalism for the ac conductance Σ_0 was properly scaled with a universal curve as per the information for $\Sigma(T, f)$ under different T . The metallic and semiconductor contribution in the dc conductivity of the doped nanosystems is highlighted. The normalized conductance (Σ/Σ_0) as a function of normalized frequency curves was depicted by a single power law for Mn-ZnO nanocapsules and nanoplates. The AC conduction process showed that x_f is a lot of phase delicate and can be utilized to describe the phase changes in these doped nanosystems originated due to change in Mn^{2+} doping concentration.

Keywords Zinc oxide nanocrystals · UV–VIS spectrum · HRTEM · Non-Ohmic conduction · Nonlinearity exponent

1 Introduction

The semiconductor zinc oxide (ZnO) is a direct and high band gap (3.37 eV) material with enormous exciton binding energy (60 meV at room temperature). In nanoscale its bandgap, optical, electrical properties can be changed significantly compared to bulk counterparts and get a lot of consideration from researchers and has a broad application in optoelectronics, different detectors, sensing, bioimaging study, lasing and many more [1–3]. One of the most

important physical properties of materials is alternating current conduction behaviour. The principle of conduction and defects that are found in crystalline solids is essentially understood by the data on the ac conductivity of semiconductors. It is well understood from current semiconductor developments that the key means of regulating electrical conductivity are the insertion of impurities or defects into semiconductor lattices which can also have an enormous impact on the optical, luminescent, magnetic, or other physical properties of the semiconductor [4]. Doping by transition metals, for example, Mn, Cr, Fe, Ni makes more distortion and defects in the nanostructure ZnO semiconductors and leads to change in ionization energy levels and tune many more properties, which can significantly modify the electrical conduction of ZnO [5, 6]. Belkhaoui et al. studied the electrical properties of Mn-doped ZnO nanoparticles [7]. Structural and optical properties of the manganese-doped ZnO have been reported by many researchers [8]. In the present study, a cost-effective approach is used for preparing manganese-doped ZnO nanocapsules (MZNC) and nanoplates (MZNP) by the simple chemical precipitation

✉ Amit Kumar Bhunia
amitphysics87@gmail.com

¹ Department of Physics, Government General Degree College at Gopiballavpur-II, Jhargram, West Bengal 721517, India

² Department of Electronics, Midnapore College (Autonomous), Midnapore, West Bengal 721101, India

³ Department of Physics, The University of Burdwan, Burdwan, West Bengal 713104, India

⁴ Department of Physics, Vidyasagar University, Paschim Medinipur, West Bengal 721102, India

technique. Moreover, the electrical and dielectric properties of ZnO nanocrystals doped with Mn^{2+} ions and others metals have been studied extensively [9–13], but nonlinear AC conduction of Mn-doped ZnO nanocapsules and nanoplates is not studied yet. Here, we motivated to study the nonlinear ac conduction in Mn-doped ZnO nanocapsules and nanoplates. Along these lines, it is essential to examine the ac conducting properties after measuring conductivity to know about the interior of semiconductor nanomaterial.

2 Experiment and instrumentations

We used different chemicals like zinc acetate ($\text{Zn}(\text{CH}_3\text{COO})_2$), manganese chloride, sodium hydroxide (NaOH) as reagents and water as a solvent for the fabrication of ZnO and Mn-ZnO nanocapsules and nanoplates. The ZnO nanocrystals are fabricated by simple wet chemical method. Firstly, 50 mL of 0.2 mol/L of zinc acetate solution was magnetically stirred for few minutes then 50 mL of 0.2 mol/L NaOH solution was added drop-wise into the $\text{Zn}(\text{CH}_3\text{COO})_2$ solution under constant magnetic stirrer at room temperature (25 °C) over a period of 30 min. Then few amounts of PVP were added during the reaction process. After three-hour reaction process, white solution with precipitation was formed. The final product was collected for characterization. In a typical manganese-doped ZnO nanocapsules (MZNC) fabrication process, 50 mL of 0.2 mol/L zinc acetate ($\text{Zn}(\text{CH}_3\text{COO})_2$) watery solution and the manganese chloride precursor (source of Mn^{2+}) in 25 mL of aqueous at 1% were added drop by drop in an air environment. To stabilize the synthesized material, a small amount of PVP (1 g in 50 ml deionized water) was added before the precursor (doping material). The mixture solution was magnetically stirred at 50 °C until it became homogeneous. Drop by drop, 50 mL of 0.2 mol/L sodium hydroxide (NaOH) solution was added to the above mixture. Following the NaOH infusion, a white voluminous precipitate appeared. The obtained dispersions were transparent and were purified several times by dialysis against deionized water and ethanol to remove impurities. The final products were dried in a hot air oven at 200 °C for 2 h. In the case of manganese-doped ZnO nanoplates fabrication, we utilize similar treatment with the same amount of reagents only the change in the added amount of manganese chloride is 25 ml aqueous at 1.5%. Transmission electron microscopy (TEM) images of the fabricated samples were used to characterize their structural and morphological properties using a JEOL JEM-2100F microscope with a 200 kV accelerating voltage. The ac conductance properties of fabricated Mn-doped ZnO nanocrystals were measured using an IM 3536 LCR METER.

The samples' optical absorption spectroscopy was recorded using a Shimadzu-Pharmaspec-1700 UV–VIS spectrometer in the wavelength range 200–900 nm. The X-ray diffraction of the powder samples was estimated in a Rigaku X-beam diffractometer using Cu-K_α radiation over the angular range (2θ) 20°–80°.

3 Results and discussions

3.1 UV–VIS spectrum and optical properties

The optical UV–VIS spectrum of the pure ZnO NPs and two different Mn-doped ZnO nanocrystals within the wavelength ranges 200–800 nm shown in Fig. 1(a). The maximum absorbance due to exciton formation arises at 372.5, 370, and 375 nm for the ZnO NPs, Mn-doped ZnO nanocapsules (MZNC), and Mn-doped ZnO nanoplates (MZNP), respectively. The shifting in the exciton wavelength is due to the tuning of band gap by Mn doping. Due to doping, some change in optical band structure leads to change in excitonic peak position as compared to pure ZnO NPs. The band gap (E_g) of the material is determined with the help of the following Tauc's equation after considering direct bandgap nature of the fabricated semiconductor material [14]:

$$(\alpha hv)^2 = c (hv - E_g).$$

Graphical plot of $(\alpha hv)^2$ vs. hv gives rise the value of E_g . The plot for three different samples is shown in Fig. 1(b)–(d). The calculated band gap is found to be 3.67, 3.45, and 3.31 eV, for the ZnO NPs, MZNC and MZNP, respectively. The resultant high band gap of ZnO NPs is matched with other reported results [15]. The reduction in band gap as of the increment of metallic Mn doping in the ZnO NPs lattice with change in ionization energy as well as change in nanocrystal sizes may tune the band gap tailoring. The bandgap of both doped nanocrystal is less than the bandgap of pure ZnO NPs. The average particle size (from HRTEM) and also crystal size (from XRD) of MZNP are greater than MZNC. So, the bandgap of MZNP is less than MZNC in the nanoscale confined region.

The Urbach energy (E_U) of the three nanocrystals has been calculated with the use of the following relation between absorption coefficient (α) and E_U [16]: $\alpha = \alpha_0 \exp [h\nu/E_u]$. The values of E_u after plotting $\ln(\alpha)$ vs $h\nu$ in the low-frequency region are found to be 0.98, 1.2, and 1.5 eV for ZnO NPs, MZNC, and MZNP, respectively. This change in the determined value of E_U may be due to change in crystal disorderness, nanocrystalline size effects and other factors.

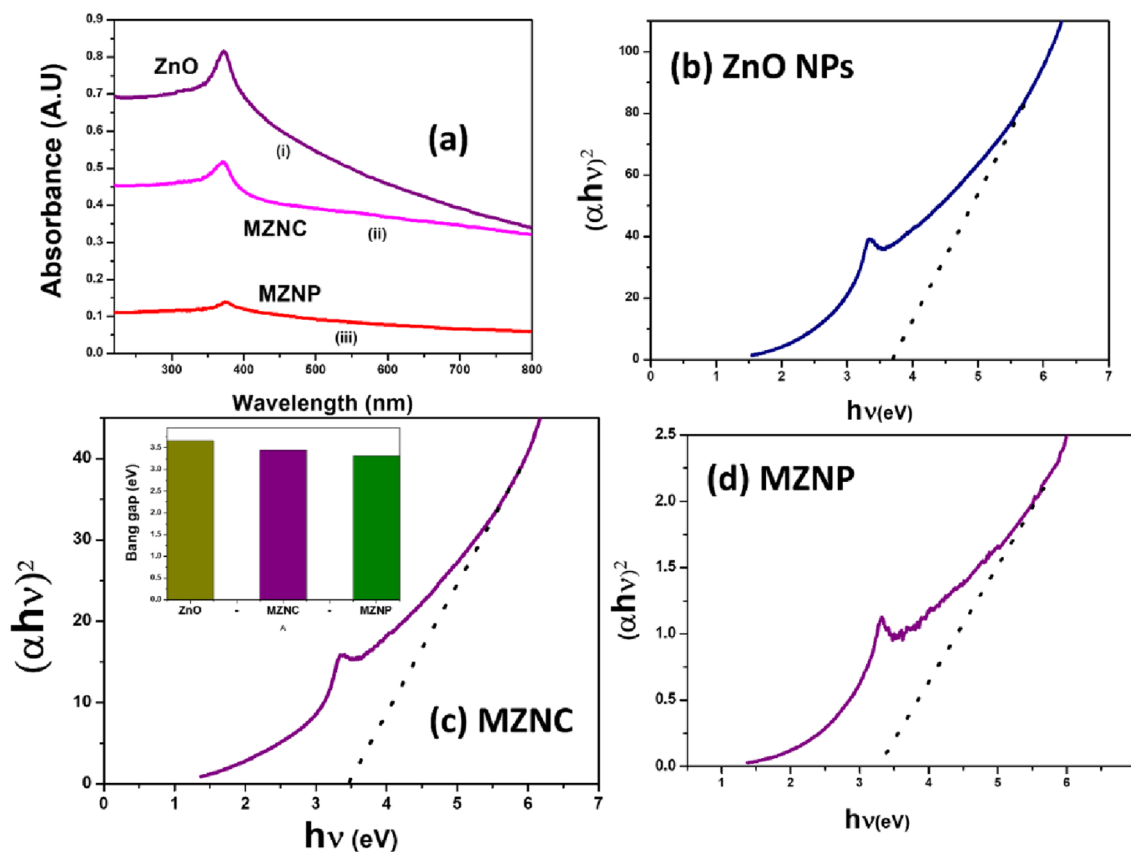


Fig. 1 a UV–VIS spectrum of (i) ZnONPs, (ii) MZNC, (iii) MZNP; Tauc’s plot for **b** ZnO NPs, **c** MZNC, **d** MZNP; inset of (c) is the histogram for the band gap of different samples

3.2 Structural properties

3.2.1 XRD study

The XRD of all samples was studied within the diffraction angle between 20 and 80°. The diffraction peaks shown in Fig. 2 show the presence of following prominent diffraction planes: (100), (002), (101), (102), (110), (103), (200), (112), (201), (004), and (202). These planes indicate the hexagonal wurtzite crystal structure of the fabricated ZnO and two Mn-doped ZnO nanocrystals [17]. As the doping concentration of Mn increases, all of the diffraction peak intensity decreases. The decrease in the diffraction peak intensity indicates more incorporation of Mn in the ZnO lattice. Mn doping occupied the lattice sites of ZnO NPs. As the ionic radius of Mn²⁺ and Zn²⁺ is different, a relative shift in the lattice constant occurs. Mn²⁺ doping increases the relative shift in lattice, which leads to decreases in scattering intensity. Scattering intensity is proportional to (structure factor)² and ‘sin’ factor. After doping both factors are decreasing, so x-ray intensity reduces. Karmakar et al. observed a decrease in x-ray scattering intensity with the increment of Mn doping in the ZnO [18]. The maximum intense diffraction peak

(101) of pure ZnO NPs at (2θ) 36.3° is shifted towards lower Bragg angles (2θ = 36.2°) with a change in peak broadening along with diffraction intensity. The observed Bragg angle shift in lattice characteristics of pure nano-ZnO could be attributed to changes in Mn concentration. The average crystal is calculated for all of the fabricated nanocrystals with the use of the following Scherrer formula [19].

$$\text{Crystalline size} : R_{hkl} = \frac{K\lambda}{\beta \cos \theta},$$

Here, K = 0.94 for Cu-K_α radiation. The average crystal size for ZnO NPs, MZNP and MZNC is found to be 35, 26, and 20 nm, respectively.

3.2.2 HRTEM

The formation of Mn-doped ZnO nanocapsules (MZNC) and Mn-doped ZnO nanoplates (MZNP) with use of 1% & 1.5% precursor is clearly observed from Fig. 3(a) & 4(a), respectively. The presence of the (100), (002), (101), (102), (110), and (103) prominent diffraction rings within the SAED pattern of Fig. 3(d) and 4(d) shows the well-crystalline

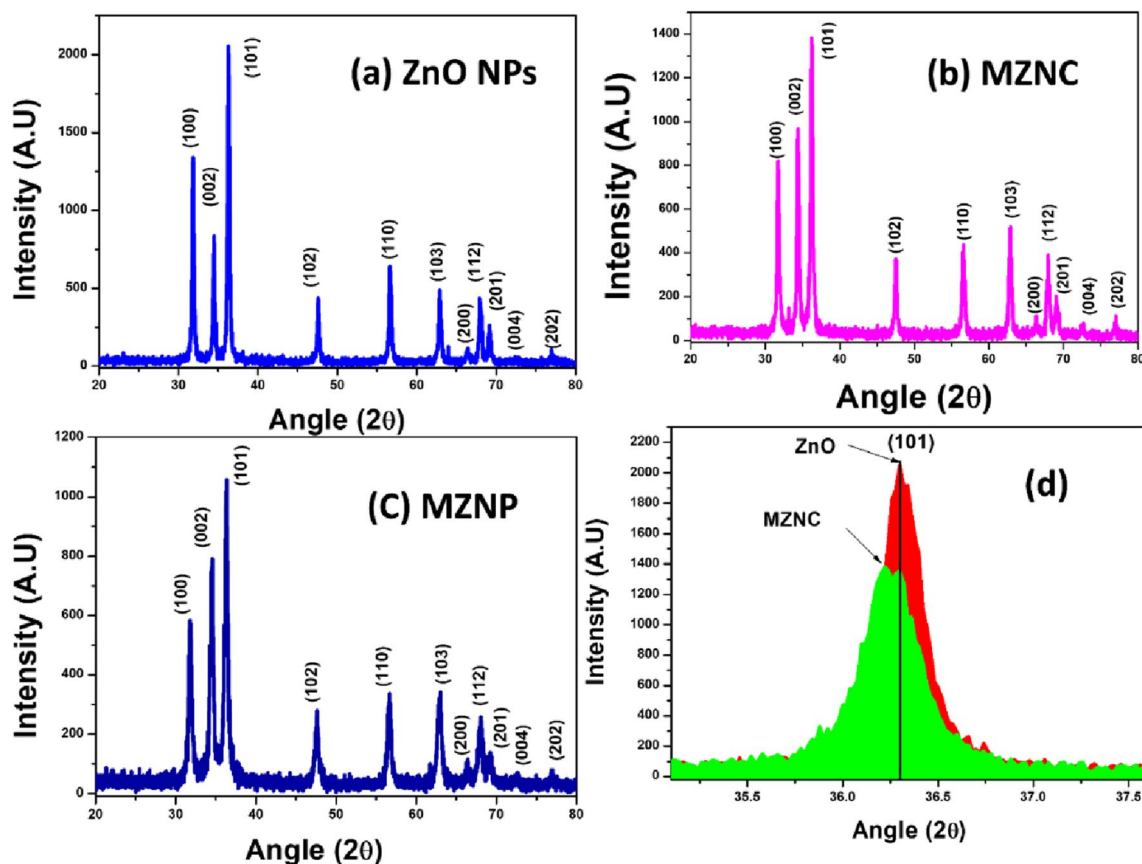


Fig. 2 XRD spectrum of **a** ZnO NPs, **b** MZNC, **c** MZNP; **d** Zoom of the (101) peak and the vertical marks indicate the position of the allowed diffraction

hexagonal wurtzite crystal phase of MZNC and MZNP, respectively. The SAED rings are well matched with the diffraction peak obtain from XRD result. The average diameter of the MZNC is ~ 29 nm, and the average length is ~ 56.5 nm. The average length of the MZNP is ~ 102 nm, and the average breadth is ~ 57 nm. Figure 3(b) shows that a bunch of nanocapsule is like a bunch of grapes. The clear image of a single nanocapsule with average diameter is ~ 27.5 nm and average length is ~ 56.5 nm as shown in Fig. 3(c). A single nanoplate with average length ~ 110 nm and breadth ~ 59.5 nm is shown in Fig. 4(c). The nanoplates are stack each other by some weak forces (Fig. 4b).

3.3 Nonlinear alternating current conduction

The ac conductance $\Sigma(T, f)$ of the pure ZnO nanocrystals, MZNC and MZNP at various temperatures was estimated as a function of frequency f with various temperatures going from 50 to 400 °C. Figure 5(a) depicts the graphical variation of estimated ac conductance ($\Sigma(T, f)$) as a function of frequency (f) in pure ZnO nanocrystals. The variation of $\Sigma(T, f)$ with f at different temperatures (T) for MZNC and MZNP is

depicted in Fig. 6(a) and (c). The conductivity in the MZNP is greater compared to MZNC for a particular temperature due to increase in manganese concentration in the ZnO NPs. The metallic manganese concentration changes the ionic energy of the semiconductor ZnO NPs, nanocrystalline size and other nanoregion effects leading to tuning of the conductivity. The real part of the ac conductance $\Sigma(P, f)$ of the deliberate Mn-doped ZnO nanosamples is nearly constant up to its Ohmic value $\Sigma(P, 0) (= \Sigma_0)$ at low frequency and deviates from Σ_0 at a specific frequency known as the onset frequency (f_c). With increasing frequency beyond f_c , $\Sigma(P, f)$ follows the power law described below [20]:

$$\Sigma(P, f) = \Sigma(P, 0) + Af^s = \Sigma_0 + Af^s, \quad (1)$$

where the exponent factor (s) is between 0 and 1, [21] and the coefficient ‘ A ’ varies with temperature in an Arrhenius manner [22, 23]. Temperature T , disorder D , and annealing time ‘ t ’ are examples of variables used to fluctuate zero-frequency zero-voltage conductance $\Sigma(P, 0) (= \Sigma_0)$. By separating the preceding expression by $\Sigma(P, f)$, one obtains [20]

Fig. 3 HRTEM image of **a** Mn-doped ZnO nanocapsules, **b** A bunch of nanocapsule, **c** Single nanocapsule, **d** SAED pattern of the nanocapsules

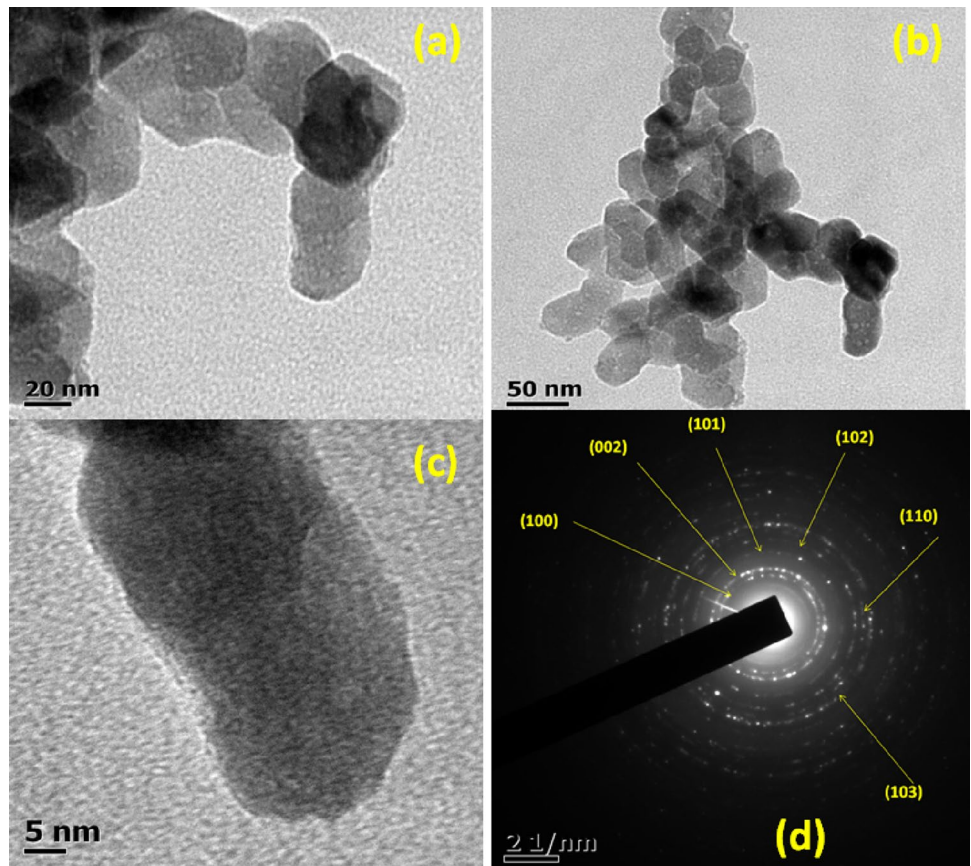
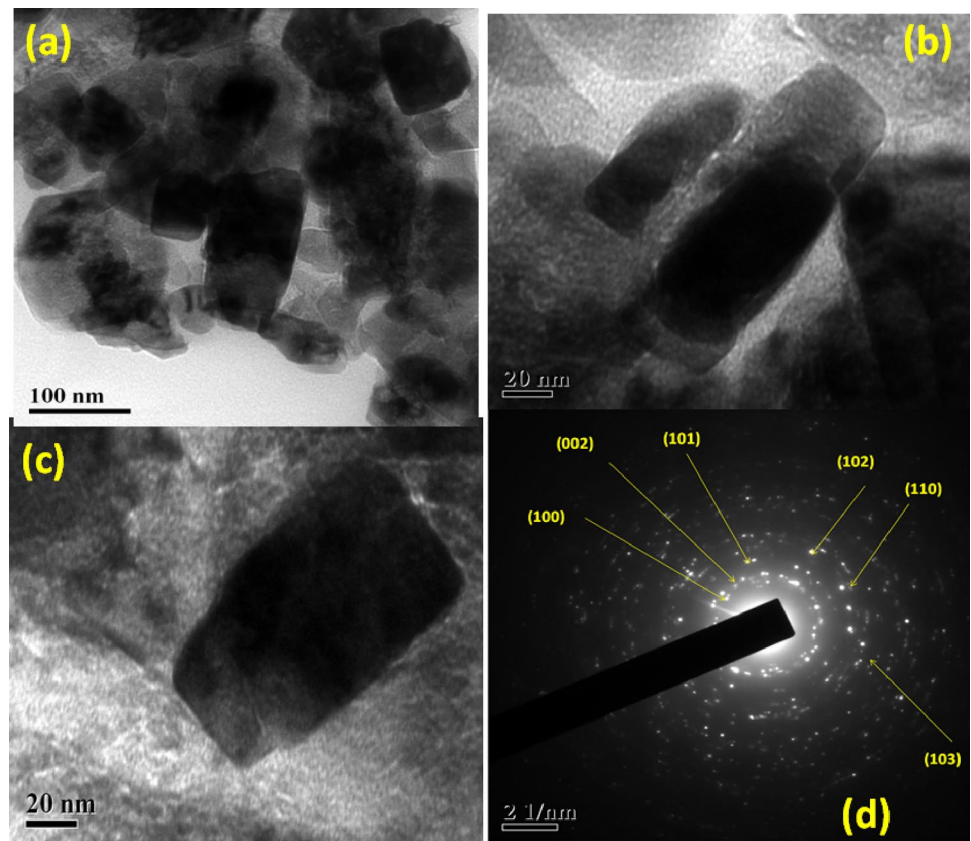


Fig. 4 HRTEM image of **a** Mn-doped ZnO nanoplates, **b** few nanoplates stage each other, **c** single nanoplate, **d** SAED pattern of the nanoplates



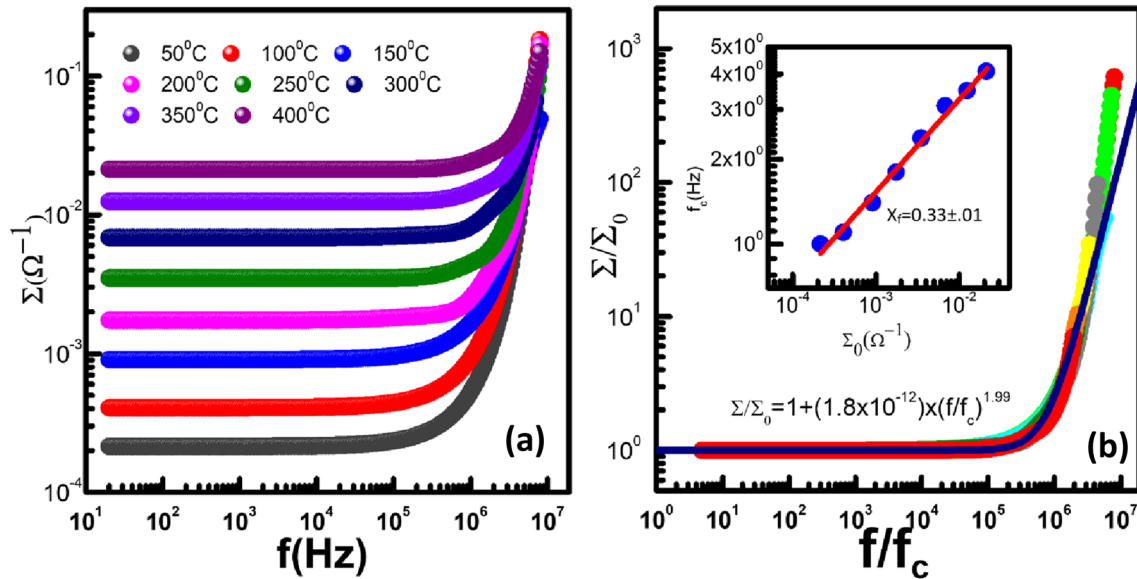


Fig. 5 **a** Variation of ac conductance $\Sigma(T, f)$ vs. frequency f in pure ZnO nanoparticles at different temperatures as indicated. **b** Scaled plot of normalized conductance $\Sigma(T, f)/\Sigma_0$ vs normalized frequency

f/f_c by varying Ohmic conductance Σ_0 by temperature T , respectively. **c** The variation of onset frequency f_c with Σ_0 . Solid line is power law fits to the data with the slopes x_f as indicated

$$\frac{\Sigma(P, f)}{\Sigma(P, 0)} = g\left(\frac{f}{f_c}\right) = 1 + Af^{x_f} \tag{2}$$

Bardhan et al. [24] have measured ac conductance at room temperature and found that f_c is solely determined by initial conductance Σ_0 . At a fixed temperature T , this onset frequency f_c scales with introductory conductivity $\Sigma(P, 0)$ as [25]

$$f_c(T) = A_T \Sigma(P, 0)^{x_f} \tag{3}$$

where $\Sigma(P, 0)$ is the same as in Eq. 1 and A_T is a constant whose value is determined by the criterion that determines the frequency scale f_c . Here, x_f is known as the nonlinearity or onset exponent and has the order of unity [25]. Above equation (Eq. 3) indicates that there exists a frequency scale in the investigated system corresponding to each value of disorder parameter. Disorder parameter may be temperature or doping [28]. The onset exponent describing the quality of nonlinearity close to the onset of nonlinear conduction. At high frequencies $f \gg f_c$, $\Sigma(P, f)$ - f curves frequently become temperature independent. The scaled conductance $\frac{\Sigma(T, f)}{\Sigma_0}$ versus scaled frequency $\frac{f}{f_c}$ results are fitted by the accompanying altered form [26, 27]

$$g(y) = 1 + By^s \tag{4}$$

where $y = \frac{f}{f_c}$, $g(y)$ is the similar scaling function in Eq. 2 and 's' is equivalent to characterized in Eq. 1. Figure 7 shows the variation of initial conductance, i.e. dc Ohmic

conductances Σ_0 versus temperature T (°C) for three samples of pure ZnO nanocrystals, MZNC and MZNP. The Σ_0 of Mn-doped ZnO nanoplates and nanocapsules decrease up to the temperature (T_t) 150.5 K and 198.5 K, respectively, and then increase with temperature. The decrease in conductivity below T_t ($T < T_t$) is due to metallic contribution in the conductivity, and the increase in Σ_0 above T_t ($T > T_t$) is due to semiconductor contribution. In case of pure ZnO nanocrystals, the value of Σ_0 increases with increase in temperature without any transition (T_t) temperature like Mn-doped ZnO (MZNC and MZNP). Hence, the behaviour of Σ_0 for pure ZnO nanocrystal semiconductor is different from that of the metal (Mn)-doped ZnO nanostructure as per our observation. This difference arises which may be due to metallic Mn doping in the ZnO lattice leading to more defect states, formation of new interstitial and lot of charge accumulation as well as formation of more mobile charges due to metallic counterparts in the semiconductor ZnO lattices. The variation of the real part of ac conductance $\Sigma(T, f)$ with frequency of the pure ZnO nanocrystals is shown in Fig. 5. In this figure we have seen only one-material phase. But the Mn-doped ZnO nanocrystals, i.e. MZNC and MZNP, show two-material phase (Fig. 6). The variation of normalized conductance $\frac{\Sigma}{\Sigma_0}$ as a function of normalized frequency f/f_c of the real component of ac conductance $\Sigma(T, f)$ of pure ZnO nanocrystals is shown in Fig. 5(b). The data collapse method analysis up to $\Sigma/\Sigma_0 \sim 500$ leads to the log-log graph of f_c vs. Σ_0 with $x_f = 0.33 \pm 0.01$ and shown in the inset of Fig. 5(b). The fitted results of Eq. (4) give $B = 1.8 \times 10^{-12}$

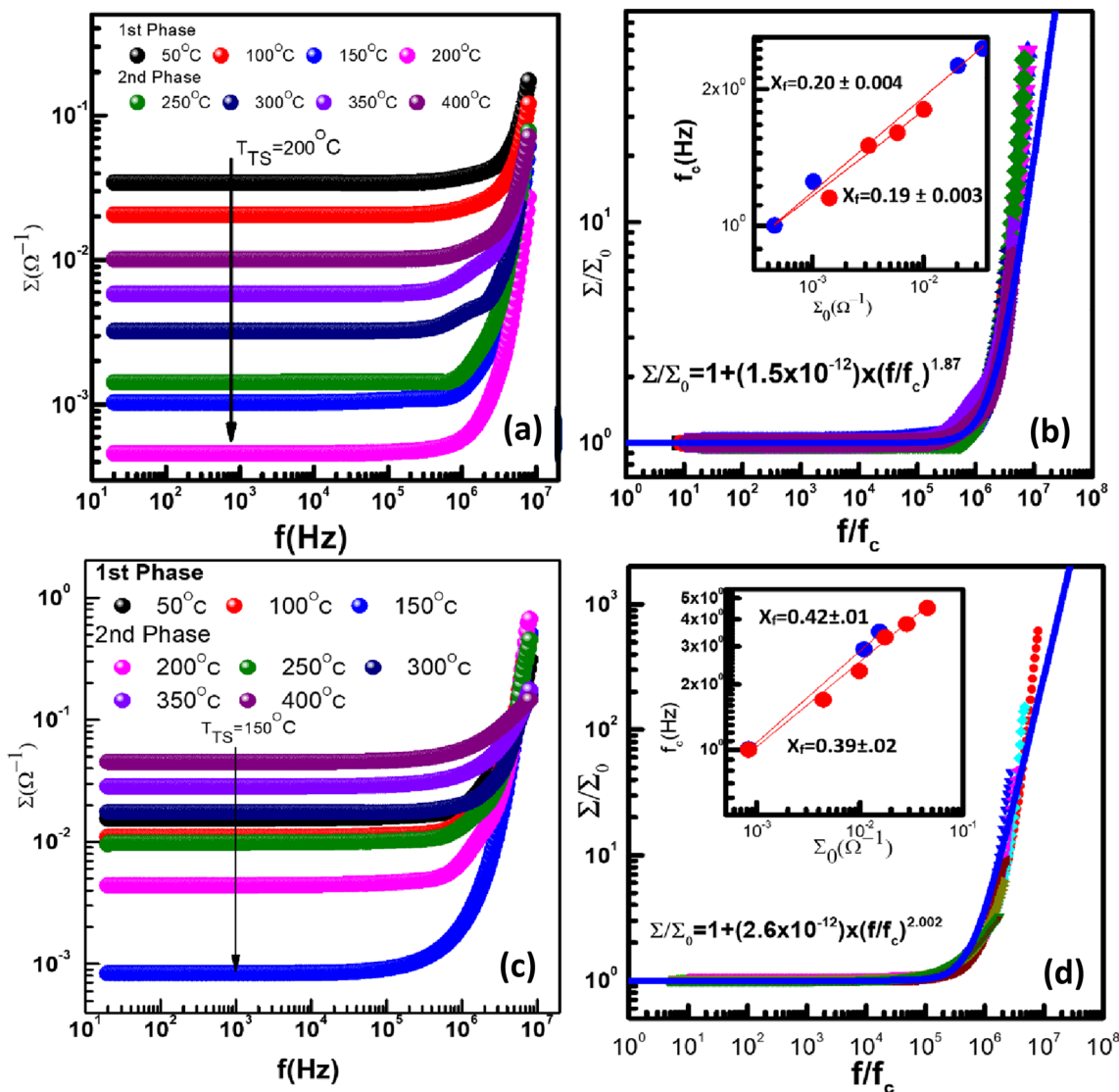


Fig. 6 a, c Variation of ac conductivity $\Sigma(T, f)$ vs. frequency f in Mn-doped ZnO nanocapsules (MZNC) and Mn-doped ZnO nanoplates (MZNP) at different temperatures as indicated. b, d Scaled plot of normalized conductivity $\Sigma(T, f)/\Sigma_0$ vs normalized frequency ff_c of

nanocapsules and nanoplates by varying Ohmic conductivity Σ_0 by temperature T , respectively. Inset of b, d shows the variation of onset frequency f_c with Σ_0 . Solid lines are power-law fits to the data with the slopes x_f as indicated

and $s = 1.99$. The variation of the real part of ac conductivity $\Sigma(T, f)$ with frequency of the MZNC and MZNP appeared in Fig. 5(a) and (c) individually at various temperatures going from 50 to 400 °C. The $\Sigma_0 - T$ graphical plot of MZNC uncovers that Σ_0 diminishes with the decline in temperature T from 200 °C and gets least at an accurate temperature T (called T_{TS}).

With more diminishing in T , Σ_0 will increment up to the deliberate temperature. Two distinct phases are observed within this variation called first phases and second phases. The region between 50 °C and T_{TS} relates to the first phase and the temperature from T_{TS} to 400 °C corresponds second phase. Comparative alternatives of $\Sigma_0 - T$ graphical

plots are determined in MZNP. The MZNC and MZNP have a zero-voltage linear conductivity $\Sigma(T, 0)$ of 0.04 S and 0.03 S for MZNC and MZNP individually at room temperature. At constant temperature, the conductivity $\Sigma(T, f)$ remains constant to its Ohmic value Σ_0 up to a precise value of frequency and then begins to expand with increasing frequency. The onset frequency f_c is the estimation of the point at which conductivity $\Sigma(T, f)$ departs from zero. It has been observed that as temperature decreases below 400 °C, Σ_0 decreases and the sample becomes non-linear at a frequency lower than that required at a higher temperature, i.e. f_c decreases with decreasing temperature

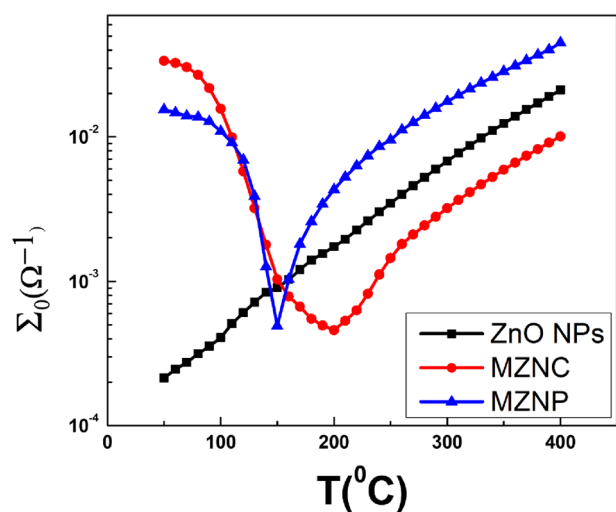


Fig. 7 The variation of DC Ohmic conductances Σ_0 versus temperature T for three samples ZnO NPs, MZNC and MZNP

up to T_{TS} . Below T_{TS} , Σ_0 increases as T decreases, and the samples exhibit non-Ohmic behaviour as f_c increases.

This convergent feature indicates that conductance at higher frequencies is completely temperature independent. The results of combining the data in Fig. 6(a) and (c) into a single curve using the data collapse method are shown in Fig. 6(b) and (d) [28, 29]. At the starting point, the minimum conductance of MZNC and MZNP at the T_{TS} , respectively, 200 °C (T_{TS}) and 150 °C (T_{TS}) was scaled by its Ohmic worth Σ_0 . As far as data collapse is concerned, any self-assertive choice (for example, 1) for f_c would suffice. For the following lower temperature in the first phase, the conductance was scaled by Σ_0 , but f_c was adjusted so that this data arrangement merged with the previous one as well as possible. The procedure was then repeated for all of the other temperatures below T_{TS} in decreasing order. In the second phase above T_{TS} , a similar procedure was used for the $\Sigma(T, f) - f$ data.

Figure 6(b) and (d) shows raw data comparisons to a variety of conductance as a function of frequency at various temperatures. The figure shows that the data scale up to $\Sigma/\Sigma_0 \sim 500$, $\Sigma/\Sigma_0 \sim 50$ and $\Sigma/\Sigma_0 \sim 500$ for pure ZnO, MZNC and MZNP, respectively, while the scaled frequency f/f_c covers seven orders of magnitude. It should be noted that the data collapse method resolves onset frequency f_c uniquely up to a constant value. The solid line in Fig. 6(b) and (d) is a fit by Eq. (4) with $B = A/\Sigma(P, 0)$, with $y = f/f_c$ and $g(y)$ as a scaling function.

The calculated values of B are 1.5×10^{-12} and 2.6×10^{-12} and s are 1.87 and 2.002 for MZNC and MZNP, respectively.

This fitting is surprisingly well within the intended frequency and conductance range, $f(c)$, which is obtained after the above model is plotted with log–log axes as

a component of the corresponding Σ_0 in the inset. The strong lines show how the power law fits to the expression $f_c \sim \Sigma_0^{x_f}$, with the exponents x_f (1st phase) = 0.33 ± 0.01 , x_f (1st phase) = 0.20 ± 0.004 and 0.42 ± 0.01 and x_f (2nd phase) = 0.19 ± 0.003 and 0.39 ± 0.002 , for single side for ZnO and both sides for MZNC and MZNP, respectively. In this investigation both of the studied exponents are positive. Results hence approve the scaling as given in Eqs. (3) and (4). Figure 6(b) and (d) suggests the log–log plot of the scaled conductance as a feature of scaled frequency for the pattern MZNC and MZNP. Figure 6(a) and (c) suggests that at a particular temperature, the actual a part of the ac conductance $\Sigma(T, f)$ in these structures stays regular as much as the function frequency and increases monotonically as frequency is accelerated beyond f_c . The scaled plots proven in Fig. 6(b) and (d) really imply the fact of a single frequency scale in any given pattern as a minimum inside the experimental tiers of frequency and conductance spanning greater than 4 orders of magnitude. The nonlinearity exponent x_f for ac conduction may be used for the identity of various phases in the investigated material systems.

4 Conclusion

The results showed that the Mn doping inside the high band gap ZnO semiconductor nanostructure tunes the different optical and structural properties. The increment of Mn doping leads to decrement of band gap with changing the crystal size and shape. We effectively clarify the phase transition and onset frequency (f_c) in pure ZnO nanocrystals and Mn-doped ZnO nanocapsules and nanoplates by considering nonlinearity exponent x_f and the real part of ac conductance $\Sigma(T, f)$. Our outcomes indicated that the positive estimation of the nonlinear exponents x_f is equal to two distinct phases with x_f (1st phase) = 0.33 ± 0.01 for ZnO NPs, x_f (1st phase) = 0.20 ± 0.004 for MZNC and 0.42 ± 0.01 for MZNP, x_f (2nd phase) = 0.19 ± 0.003 for MZNC and 0.39 ± 0.002 for MZNP in both sides of the observed onset frequency. The discussion showed that the normalized conductance Σ/Σ_0 are perfectly obeys a single-power law with the values of $\Sigma/\Sigma_0 \sim 500$ and $\Sigma/\Sigma_0 \sim 50$ and $\Sigma/\Sigma_0 \sim 500$ for pure ZnO nanocrystals, MZNC and MZNP, respectively. The result of the variation of the real part of ac conductance with frequency showed pure ZnO nanocrystals was in one-material phase, whereas the Mn-doped ZnO nanocrystals, i.e. MZNC and MZNP, were two-material phase. The experimental result fitted by theoretical model to study nonlinear ac conduction mechanism and phase change behaviour of Mn-doped ZnO nanocapsules and nanoplates compared with pure ZnO NPs is a new direction of research to understand better inside the composite semiconductors and its various electrical applications. The ac conduction nonlinearity

exponent x_f can be used to identify different phases in the investigated undoped and metal-doped nanoscale semiconductor material systems.

Acknowledgements The authors are grateful to the Department of Physics of Vidyasagar University. The author AKB is thankful to the Department of Physics, Government General Degree College at Gopiballavpur-II. The author AKB is thankful to the CRF, IIT Kharagpur.

Author contributions AKB and SS assisted the problem of the research, carried out the measurement and manuscript writing. AKB and TNG, KB assisted the measurement, discussed and helped draft the manuscript. All authors read and approved the final manuscript.

Funding Author AKB is thankful to Dept. of Higher Education, Science and Technology and Biotechnology, Government of West Bengal, India.

Data availability All data that support the findings of this study are included within the article.

Declaration

Competing interests The authors declare that they have no competing interests.

References

- H.M. Xiong, Y. Xu, Q.-G. Ren, Y.-Y. Xia, *J. Am. Chem. Soc.* **130**, 7522 (2008)
- F. Bagheri, H. Haratizadeh, *Mater. Sci. Semicond. Process.* **141**, 106422 (2022)
- M. Belhaj, C. Dridi, H. Elhouichet, J.C. Valmalette, *J. Appl. Phys.* **119**, 095501 (2016)
- F. Abrinaei, N. Molahasani, *J. Optical Soc. Am. B* **35**(8), 2015 (2018)
- M. Nirmala, A. Anukaliani, *Mater. Lett.* **65**, 2645 (2011)
- J. Zhong, S. Muthukumar, Y. Chen, Y. Lu, H.M. Ng, W. Jiang, E.L. Garfunkel, *Appl. Phys. Lett.* **83**, 3401 (2003)
- C. Belkhaoui, R. Lefi, N. Mzabi, H. Smaoui, *J. Mater. Sci.: Mater. Electron.* **29**, 7020 (2018)
- D. Sharma, R. Jha, *J. Alloy. Compd.* **698**, 532 (2017)
- M.H. Zulfqar, M. Zubair, A. Khan, T. Hua, N. Ilyas, S. Fashu, A.M. Afzal, M.A. Safeen, R. Khan, *J. Mater. Sci. Mater. Electron.* **32**, 9463–9474 (2021)
- H. Saadi, Z. Benzarti, P. Sanguino, Y. Hadouch, D. Mezzane, K. Khirouni, N. Abdelmoula, H. Khemakhem, *Appl. Phys. A* **128**, 691 (2022)
- V.D. Mote, Y. Purushotham, B.N. Dole, *Mater. Des.* **96**, 99 (2016)
- C. Belkhaoui, N. Mzabi, H. Smaoui, *Mater. Res. Bull.* **111**, 70 (2019)
- D. Zhang, *Russ. J. Phys. Chem. A* **86**(1), 93 (2012)
- A.K. Bhunia, S. Saha, *Luminescence* **36**, 149 (2021)
- A.K. Bhunia, P.K. Jha, S. Saha, *Luminescence* **37**, 892 (2022)
- S. Benramache, B. Benhaoua, H. Bentrach, *J. Nanostr. Chem.* **3**, 1 (2013)
- Z.R. Tian, J.A. Voigt, J. Liu, B. Mckenzie, M.J. Mcdermott, M.A. Rodriguez, H. Konishi, H. Xu, *Nat. Mater.* **2**, 821 (2003)
- R. Karmakar, S.K. Neogi, A. Banerjee, S. Bandyopadhyay, *Appl. Surf. Sci.* **263**, 671 (2012)
- A.K. Bhunia, T. Kamilya, S. Saha, *Chem. Select* **1**, 2872–2882 (2016)
- A.K. Bhunia, T.N. Ghosh, *J. Mater. Sci.* **33**, 17963 (2022)
- J.C. Dyre, T.B. Schroder, *Rev. Mod. Phys.* **72**, 873 (2000)
- W.K. Lee, J.F. Liu, A.S. Nowich, *Phys. Rev. Lett.* **67**, 1559 (1991)
- A.S. Nowick, A.V. Vaysleyb, B.S. Lim, *J. Appl. Phys.* **76**, 4429 (1994)
- K.K. Bardhan, R.K. Chakrabarty, *Phys. Rev. Lett.* **72**, 1068 (1994)
- T.N. Ghosh, U.N. Nandi, S. Chattopadhyay, D. Jana, S.C. Saha, *Solid State Commun.* **152**, 1595 (2012)
- U.N. Nandi, S. Sircar, A. Karmakar, S. Giri, *J. Phys. Condens. Matter* **24**, 265601 (2012)
- D. Chakraborty, U.N. Nandi, D. Jana, Md.G. Masud, S. Giri, *J. Appl. Phys.* **118**, 035103 (2015)
- U.N. Nandi, Y.Z. Long, D. Chakraborty, *Results Phys.* **3**, 84 (2013)
- D. Talukdar, U.N. Nandi, K.K. Bardhan, C.C. Bufon, T. Heinzl, A. De, C.D. Mukherjee, *Phys. Rev. B* **84**, 054205 (2011)

Publisher's Note Springer Nature remains neutral with regard to jurisdictional claims in published maps and institutional affiliations.

Springer Nature or its licensor (e.g. a society or other partner) holds exclusive rights to this article under a publishing agreement with the author(s) or other rightsholder(s); author self-archiving of the accepted manuscript version of this article is solely governed by the terms of such publishing agreement and applicable law.